SrGAP3 interacts with lamellipodin at the cell membrane and regulates Rac-dependent cellular protrusions

Volker Endris[1], Lydia Haussmann[1], Elena Buss[1], Claire Bacon[1], Dusan Bartsch[2] and Gudrun Rappold[1,*]

[1]Department of Human Molecular Genetics, University of Heidelberg, Germany
[2]Department of Molecular Biology, Central Institute of Mental Health and University of Heidelberg, Mannheim Medical Faculty, Mannheim, Germany
*Author for correspondence (gudrun_rappold@med.uni-heidelberg.de)

Accepted 13 June 2011
Journal of Cell Science 124, 3941–3955

doi: 10.1242/jcs.077081

Summary

SrGAP3/MEGAP is a member of the Slit–Robo GAP (srGAP) family and is implicated in repulsive axon guidance and neuronal migration through Slit–Robo-mediated signal transduction. Here we describe an inhibitory role of srGAP3 on actin dynamics, specifically on lamellipodia formation. We show that the F-BAR domain localizes srGAP3 to the leading edge of cellular protrusions whereas the SH3 domain is important for focal adhesion targeting. We report on a novel srGAP3 interaction partner, lamellipodin, which localizes with srGAP3 at the leading edge. Live-cell analyses revealed that srGAP3 influences lamellipodin-evoked lamellipodial dynamics. Furthermore, we show that mouse embryonic fibroblasts derived from homozygous srGAP3-knockout embryos display an increased cell area and lamellipodia formation that can be blocked by shRNA-mediated knockdown of lamellipodin.

Key words: Actin dynamics, F-BAR, Focal adhesions, Slit–Robo signaling

Introduction

The members of the Slit–Robo GAP family (srGAP1–srGAP3) are GTPase-activating proteins that share a common molecular architecture, consisting of an N-terminal F-BAR domain, a centrally located GAP and an Src homology 3 (SH3) domain (Wong et al., 2001; Endris et al., 2002; Soderling et al., 2002; Guerrier et al., 2009). The SH3 domain of all three members has been shown to interact with the intracellular part of the Robo1 receptor (Wong et al., 2001). Robo1 and its ligand Slit are involved in a variety of developmental processes including neuronal migration and steering of axonal projections (Brose et al., 1999; Nguyen-Ba-Charvet and Chédotal, 2002; Hohenester, 2008). Binding of Slit to its receptor has been shown to initiate a signaling cascade involving srGAP1, leading to downregulation of the small GTPase Cdc42 and activation of RhoA (Wong et al., 2001). This is believed to lead to a local destabilization of the actin cytoskeleton necessary for repulsive axon guidance or cell migration (Geraldo and Gordon-Weeks, 2009). Although srGAP1 downregulates Cdc42, the GAP domains of both srGAP2 and srGAP3 are specific for Rac1 (Endris et al., 2002; Soderling et al., 2002; Yang et al., 2006; Guerrier et al., 2009). srGAP3, which is also called MEGAP or WRP, is widely expressed in the developing brain and is implicated in the etiology of cognitive impairment (Endris et al., 2002; Bacon et al., 2009). In neuroblastoma cells, expression of srGAP3 leads to cell rounding and impaired cell migration as a result of downregulation of Rac1 signaling (Yang et al., 2006) and its inhibitory role on WAVE1 (Soderling et al., 2002). Rac1 and its downstream target WAVE1 play an essential role in the formation of lamellipodia in fibroblasts and regulate neuronal morphology (Hall, 1998; Eden et al., 2002; Stradal and Scita, 2006). The interplay of srGAP3 and WAVE1 furthermore is important for the development of dendritic spines in primary hippocampal neurons (Soderling et al., 2007; Carlson et al., 2011). Through its F-BAR domain, srGAP2 regulates the rate of neuronal migration in the forebrain and branching of leading processes (Guerrier et al., 2009). The F-BAR (or EFC) domain, which constitutes a novel type of membrane binding domain, can be found in a variety of different proteins, such as FBP17, CIP4 and FES (Tsujita et al., 2006; McPherson et al., 2009; Toguchi et al., 2010). F-BAR domains form elongated α-helical coils that bind to the membrane as homodimers (Shimada et al., 2007). Through their slightly curved structure, they lead to a bending of the membrane, which, depending on the orientation of the curvature, can be a priming process for either vesicle formation or induction of filopodia (Itoh and De Camilli, 2006). In COS7 fibroblasts, expression of the full-length F-BAR domain of srGAP2 and srGAP3 alone is sufficient to induce filopodia (Guerrier et al., 2009; Carlson et al., 2011), whereas deletion of the last 49 amino acids abolishes this effect but still localizes the protein to the cell membrane. The dynamics of filopodia rely mainly on actin polymerization through members of the Ena/VASP or formin family (Applewhite et al., 2007; Drees and Gertler, 2008; Mellor, 2010). Ena/VASP proteins localize to the leading edge of lamellipodia and filopodia, and regulate the length and branching density of actin filaments (Krause et al., 2003; Tokuo and Ikebe, 2004). After their recruitment to receptor–signaling complexes at the membrane, Ena/VASP proteins cooperate with other proteins in regulating lamellipodial protrusion (Bashaw et al., 2000; Yu et al., 2002). One of these proteins is lamellipodin, which has been shown to directly interact with Ena/VASP proteins at the tips of filopodia

and protruding lamellipodia (Krause et al., 2004), thereby regulating actin dynamics. The activity of lamellipodin can be regulated by c-Abl-mediated phosphorylation, which increases its interaction with Ena/VASP proteins downstream of PDGF and which in neurons is important for axonal morphogenesis (Michael et al., 2010).

Here, we report on the inhibitory role of srGAP3 on formation of lamellipodia and focal adhesions. We provide evidence that srGAP3 is targeted to sites of lamellipodia formation through its F-BAR domain, whereas localization at focal adhesions requires an intact SH3 domain. In a screen for novel SH3 binding partners, we identified the Ena/VASP binding protein lamellipodin. We show that srGAP3 is co-expressed with lamellipodin in the brain and that both proteins interact. SrGAP3 colocalizes with lamellipodin at the cellular membrane and interferes with lamellipodin-evoked actin dynamics. Mouse embryonic fibroblasts isolated from *Srgap3*$^{-/-}$ animals present increased lamellipodia formation, which can be blocked by knockdown of lamellipodin. In N1E-115 neuroblastoma cells, srGAP3 and lamellipodin cooperate in a common pathway to regulate the induction of neurite-like processes.

Results

F-BAR and SH3-mediated localization of srGAP3 to the membrane and focal adhesions

We previously demonstrated that the expression of srGAP3 strongly influences the cell cytoskeleton by impairing Rac1 activity. SHSY-5Y neuroblastoma cells stably expressing srGAP3 displayed a rounded morphology and an impaired cell migration rate (Yang et al., 2006). We have now analyzed in more detail the influence of srGAP3 on the actin cytoskeleton using live imaging and total internal reflection microscopy (TIRF) to investigate the dynamic localization of srGAP3 in the cell with EYFP-tagged constructs. Expression of srGAP3–EYFP in mouse fibroblasts (NIH3T3) or B16-F1 mouse melanoma cells resulted in a similar cell-rounding effect as observed for SHSY-5Y neuroblastoma cells. Compared with EYFP control cells, which frequently formed lamellipodia, srGAP3-expressing cells only formed small protrusions, were not dynamic and did not adhere properly (Fig. 1A; supplementary material Movie 1). By contrast, the expression of a GAP-deficient mutant of srGAP3 (R542I), which is unable to downregulate Rac1 (Yang et al., 2006), restored the dynamic behavior of the cells, which formed lamellipodia and had a flattened morphology (Fig. 1B; supplementary material Movie 2). Quantitative analysis of the total cell area showed that srGAP3-expressing cells were significantly smaller compared with EYFP control cells (srGAP3, 1167.76 μm^2; $n=108$; EYFP, 1600.25 μm^2; $n=103$; $P<0.01$), whereas cells expressing the GAP mutant srGAP3 were similar in size to control cells (R542I, 1696.45 μm^2; $n=115$) (Fig. 1E). Similarly, coexpression of srGAP3 with constitutive-active Rac1 restored lamellipodia formation and adhesion properties (Fig. 1C; supplementary material Movie 3). Corresponding to its role in inhibiting the formation of lamellipodia, wild-type srGAP3 showed localization at the cell membrane, especially around the tips of small protrusions and at the tips of small filopodia. Similarly to wild-type srGAP3 protein, the GAP mutant also localized to the cell membrane, in particular to the leading edges of lamellipodia (Fig 1A,B). Staining of endogenous srGAP3 in mouse embryonic fibroblasts (MEFs) and NIH3T3 cells using two different polyclonal antibodies showed a punctate staining pattern in the cell cytosol and at the leading edge of lamellipodia (Fig 1F). Co-staining with Phalloidin–TRITC, which labels filamentous actin, showed that these srGAP3-positive dots were mainly localized in areas with low F-actin content. A quantitative measurement of the distribution of srGAP3 dots along the leading edge indeed showed that 80.31% were located in regions where the intensity of the F-actin staining was diminished (supplementary material Fig. S1). Similar results were obtained for both antibodies tested, whereas control staining using either secondary antibodies alone or staining of *Srgap3*$^{-/-}$ MEFs did not show a clustered localization of signals (data not shown). Similarly to fibroblasts, the staining of srGAP3 in stage 2–3 primary mouse cortical neurons was punctate throughout the soma–neurite compartment, as well as in the growth cone (Fig. 1G).

srGAP3 contains an F-BAR domain at its N-terminus, followed by a GAP and SH3 domain (Fig. 2D). F-BAR domains have been previously shown to bind to cell membranes and to induce a bending of the membrane (Heath and Insall, 2008). In particular, the F-BAR domain of the srGAP protein family has been described to be important for membrane localization and filopodia induction in COS7 cells (Guerrier et al., 2009; Carlson et al., 2011). To analyze whether the F-BAR domain of srGAP3 is responsible and necessary to recruit srGAP3 to the cell membrane of NIH3T3 cells, we used an N-terminally-truncated srGAP3 construct. In contrast to wild-type srGAP3, the ΔF-BAR construct did not show any membrane localization, indicating that the F-BAR domain is also important for membrane targeting of srGAP3 in NIH3T3 cells (Fig. 2A). Because srGAP3-expressing cells lack leading edge lamellipodia, we also tested the ΔF-BAR construct in a GAP-deficient backbone to confirm that the ΔF-BAR srGAP3 construct does not localize to the leading edge (supplementary material Movie 4). By contrast, the expression of the isolated F-BAR domain of srGAP3 alone was sufficient for membrane targeting, although the staining pattern was more punctuate and not closely restricted to lamellipodial leading edges (Fig. 2B; supplementary material Movie 5) and was not changed upon co-expression of constitutive-active Rac1 (Fig. 2C).

The F-BAR domains of srGAP2 and of srGAP3 have been described to induce filopodia in COS7 cells and primary cortical neurons (Guerrier et al., 2009; Carlson et al., 2011). They also showed that the last 49 amino acids of the F-BAR domain define its ability to form filopodia, whereas the rest of the domain only acts as a membrane-targeting motif. In srGAP3, part of these 49 amino acids are encoded by exon 12, which can be alternatively spliced (Endris et al., 2002), leading to the isoforms srGAP3a and srGAP3b. We tested both isoforms in NIH3T3 and B16-F1 cells, but none of these two splice forms was able to induce filopodia (data for b-form not shown). Because the experiments with srGAP2 have been performed in COS7 cells, we also tested srGAP3 in this cell line.

Similarly to NIH3T3 cells, COS7 cells expressing srGAP3 did not display dynamic protrusions or lamellipodia. Instead, the cells presented numerous short, actin-rich structures, that were similar to the outward protrusions described for the IF-BAR domains. These structures were seen for both srGAP3a (supplementary material Fig. S2B) and srGAP3b (supplementary material Fig. S2C), but not in EYFP control cells (supplementary material Fig. S2A). We next tested the ability of the isolated F-BAR domain of srGAP3 to induce outward protrusions. Our results show that the

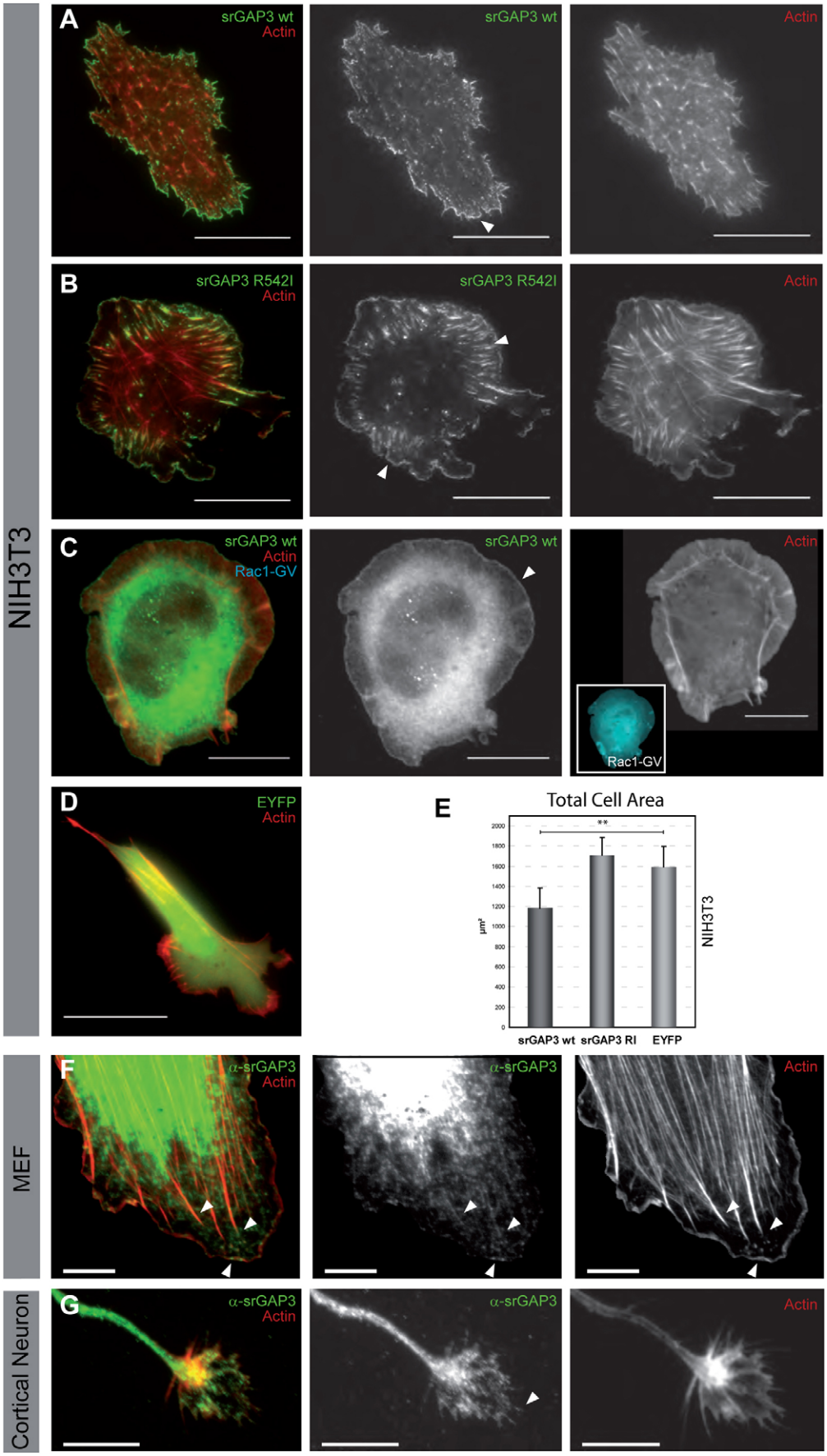

Fig. 1. srGAP3 localizes to lamellipodia and influences cell morphology. (**A**) TIRF image of an NIH3T3 fibroblast cell plated on fibronectin transfected with wild-type srGAP3–EYFP and mRFP–actin. Cells expressing wild-type srGAP3 are not dynamic and have lower adhesion properties. Note the prominent localization of srGAP3 distal to F-actin in small protrusions at the cell membrane and in small filopodia, and the lack of lamellipodia. (**B**) Cell transfected with the GAP-deficient srGAP3–EYFP construct (R542I) showing prominent lamellipodia. srGAP3-R542I localizes at the leading edge of lamellipodia and at the ends of actin fibers (arrowheads). (**C**) Epifluorescence image of an NIH3T3 cell coexpressing srGAP3 with constitutive-active Rac1 (G12V), which rescues lamellipodia formation. Note the localization of wild-type srGAP3 at the leading edge of lamellipodia (arrowhead). (**D**) Epifluorescence image of an EYFP control NIH3T3 cell plated on fibronectin. (**E**) Quantitative analysis of the total cell area of srGAP3 or EYFP control cells. Wild-type srGAP3 cells are smaller as a result of diminished adhesion properties and lack of protrusions ($n>100$ each; mean ± s.e.m.). The GAP-deficient R542I mutation rescues this effect and these cells do not differ from control cells. (**F**,**G**) Immunofluorescence staining of endogenous srGAP3. Mouse embryonic fibroblasts were immunostained with a specific srGAP3 antibody and counterstained with Phalloidin-TRITC to visualize the actin cytoskeleton (F). Endogenous srGAP3 localizes to the leading edge of lamellipodia in a distinct punctate staining pattern and does not overlap with F-actin (arrowheads) and in discrete lines along actin stress fibers. In the growth cone of a mouse cortical neuron (DIV4), srGAP3 colocalizes with actin-rich structures and can be found at the tips of filopodia (G, arrowhead). Scale bars: 25 µm (A–D), 10 µm (F,G).

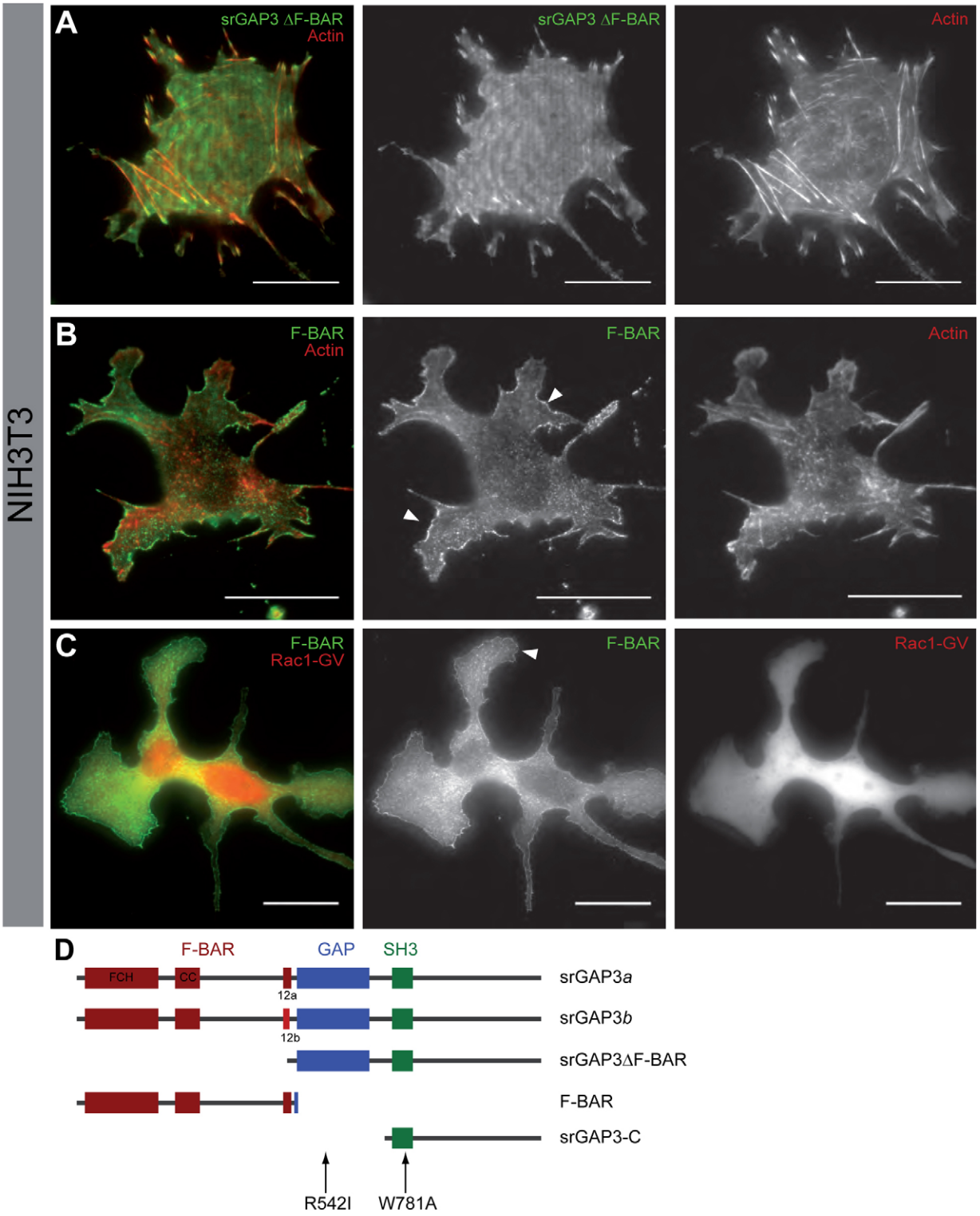

Fig. 2. The F-BAR domain of srGAP3 is important for membrane localization. (**A**) TIRF image of an NIH3T3 cell expressing srGAP3ΔFBAR. The deletion of the N-terminal F-BAR domain abolishes the membrane binding of srGAP3. The srGAP3ΔF-BAR construct mainly distributes in the cytoplasm, but not at the cell membrane. No change is observed in its localization at the ends of actin fibers. (**B**) The F-BAR domain alone is sufficient for membrane localization (arrowhead). In addition, the F-BAR construct clusters in vesicular structures within the cytoplasm. (**C**) Coexpression of the F-BAR domain with constitutive-active Rac1 (G12V) showing its localization at the rim of large protrusions (arrowhead). (**D**) Schematic presentation of the srGAP3 domain architecture and the introduced mutations. srGAP3*a* and srGAP3*b* represent splice variants differing in the alternative use of exon 12, which constitutes a part of the F-BAR domain. F-BAR, FCH-BAR homology domain; FCH, Fes-CIP4 homology region; CC, coiled coil region; GAP, GTPase-activating domain; SH3, Src homology 3 domain. R542 and W781 are highly conserved residues in the GAP or SH3 domains that are important for domain properties. Scale bars: 25 μm.

F-BAR domain of srGAP3 alone does not promote the formation of filopodia, but we observed the formation of small, microspike-resembling structures that might be an indication for the described outward membrane bending activity of IF-BAR domains (supplementary material Fig. S2D). Interestingly, cells expressing the GAP-deficient R542I mutant (supplementary material Fig. S2F) did not present outward protrusions, but rather had a smooth surface. We therefore tested the effect of Rac1 in the formation of the observed structures. Indeed, expression of dominant-negative Rac1 (T17N) also led to the formation of short actin projections (supplementary material Fig. S2G), whereas coexpression of srGAP3a with constitutive-active Rac1 (G12V) restored lamellipodia formation and prevented the formation of projections (supplementary material Fig. S2H). Similarly, expression of an F-BAR-deleted srGAP3 construct also resulted in cells expressing short actin projections (supplementary material Fig. S2E). Taken together, our results suggest that the interplay of the F-BAR domain of srGAP3 and the GAP-dependent downregulation of Rac1 might facilitate the formation of actin-rich projections at the cell surface in COS7 cells.

As well as localizing to the cell periphery, TIRF analysis showed that the wild type, the GAP-deficient and the F-BAR-deleted constructs of srGAP3 also localize to structures at the underside of the cell in the periphery of small protrusions and to lamellipodia. A closer look at these sites revealed that srGAP3 was localized at the end of actin stress fibers, which eventually terminate in focal adhesions (supplementary material Fig. S3A,B). Indeed, co-staining of srGAP3 with vinculin, a marker for focal adhesions, showed a large overlap of both proteins, with srGAP3 localizing more distally compared with vinculin (supplementary material Fig. S3C,D).

Focal adhesions are composed of many different proteins that often interact through SH2- and SH3-dependent mechanisms. srGAP3 contains an SH3 domain at its C-terminus. To determine whether the localization of srGAP3 at focal adhesions requires an intact SH3 domain, we introduced a point mutation at a highly conserved amino acid residue within the SH3 binding groove (W781A) (Soderling et al., 2002). In contrast to wild-type srGAP3, the SH3 mutant showed no staining at the ends of actin filaments, independently of the GAP activity (supplementary material Fig. S4A,B) or at vinculin-positive focal adhesions (supplementary material Fig. S4D). In addition, we observed a reduced, but not completely abolished binding to the cell membrane, suggesting that the SH3 domain contributes to localization at the leading edge. Introduction of the SH3 mutation into the ΔF-BAR construct resulted in an srGAP3 mutant that did not bind to either the membrane or focal adhesions (supplementary material Fig. S4C). Furthermore, expression of the srGAP3 C-terminus alone, containing the SH3 domain (for scheme see Fig. 2D) was sufficient for colocalization with actin fibers (supplementary material Fig. S5A) and this colocalization was disturbed by introducing the W781A SH3 mutation (supplementary material Fig. S5B). Similar results could also be obtained using the isolated SH3 domain of srGAP3 fused to EGFP (supplementary material Fig. S5C–E). These results indicate that srGAP3 uses two protein domains for proper localization within the cell. Although the F-BAR domain is a prerequisite for membrane targeting, the SH3 domain helps to localize srGAP3 to focal adhesions. The observed reduction in membrane staining for the SH3 mutant suggests that the SH3 domain might also participate in the functioning of srGAP3 at the membrane.

Considering that srGAP3 localizes to focal adhesions and that cells expressing srGAP3 have a reduced ability to properly adhere, we investigated the possible influence of srGAP3 on focal adhesions. We stained cells expressing wild-type or mutant srGAP3 with vinculin and visualized the cells using TIRF microscopy. Quantification of the vinculin-positive focal adhesions revealed that cells expressing wild-type srGAP3 had a ~40% decrease in focal adhesion area compared with that in EYFP-expressing control cells ($n=102$; $P<0.0001$) (supplementary material Fig. S3E). By contrast, cells that expressed the GAP-deficient R542I mutant had a slightly increased focal adhesion area, indicating that the GAP activity of srGAP3 principally determines focal adhesion formation ($n=107$; $P=0.0045$). Because the SH3 domain of srGAP3 is important for its targeting to focal adhesions, we also analyzed the SH3 mutant W781A. Compared with the reduced area of wild-type srGAP3-expressing cells, the area of focal adhesions in cells expressing the W781A mutant was increased ($n=109$; $P=0.0047$), but still smaller than in EYFP control cells ($P=0.0005$), which is probably due to the intact GAP activity. The increase in focal adhesion area was mainly caused by a change in the number of focal adhesions, but not by a change in the average size of the focal adhesions (EYFP, 26.51; srGAP3 wt, 12.49; R542I, 30.7; W781A, 16.68; $n>100$) (supplementary material Fig. S3E).

srGAP3 interacts with lamellipodin

srGAP3 has been shown to interact with Robo1 (Wong et al., 2001) and WAVE1 (Soderling et al., 2002), proteins involved in Slit–Robo-mediated axon guidance and actin dynamics. To further elucidate the role of srGAP3 in regulating cytoskeletal dynamics at the leading edge, we sought to identify novel proteins that could link srGAP3 to the actin machinery.

Because of the role of SH3 domains in protein–protein interactions, we performed GST pull-down experiments using the srGAP3 SH3 domain, followed by mass spectrometry. Subsequent analysis of srGAP3 SH3-specific bands, which were not detected with GST alone, revealed components of the WAVE1 complex (WAVE1, PIR121, NAP1) that are known to be associated with srGAP3 (Soderling et al., 2002) (supplementary material Fig. S6). In addition to the WAVE complex, the MS data from two independent experiments identified a putative novel srGAP3 interaction partner, lamellipodin (Lpd), which has been identified as a Ena/VASP binding protein implicated in lamellipodial dynamics (Krause et al., 2004). Next, we sought to confirm this interaction using pull-down and immunoprecipitation experiments. First, we used GST pull-downs using the srGAP3 SH3 domain to precipitate Myc-tagged lamellipodin from HEK293 cell lysates. We were able to detect the Myc-tagged lamellipodin in the srGAP3 SH3 precipitates, but not in GST controls (not shown).

We then aimed to investigate whether srGAP3 and lamellipodin form protein complexes in the cell. We performed co-immunoprecipitation experiments using HEK293 cells transfected with expression constructs for srGAP3 and Myc-tagged lamellipodin, showing the binding of wild-type srGAP3 protein to lamellipodin (Fig. 3A). As a specificity control, we included two SH3 domain mutants, W781A and Y755D. In contrast to the wild type, the two srGAP3 SH3 mutants did not

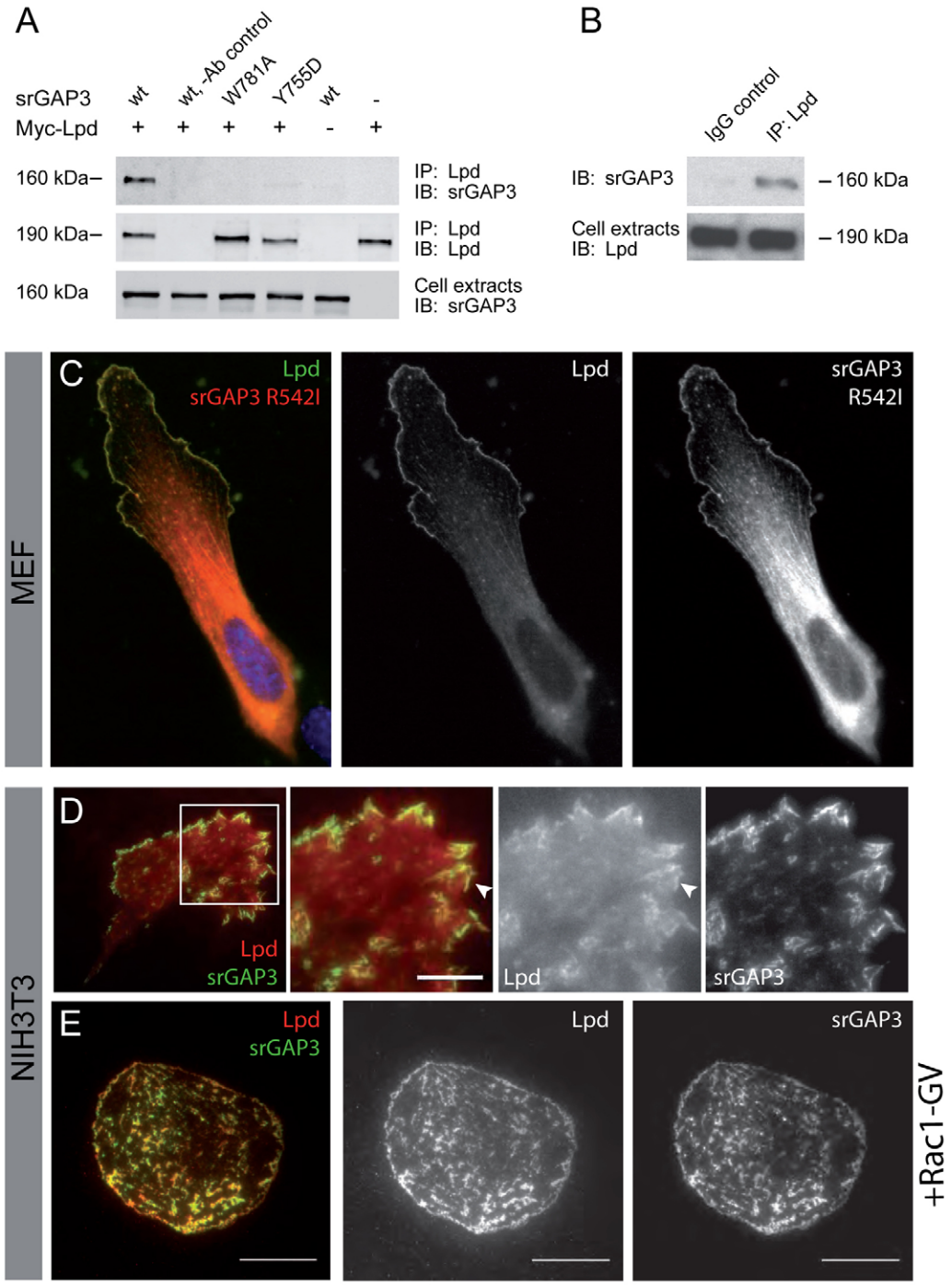

Fig. 3. srGAP3 binds to lamellipodin. (**A**) HEK293 cells were co-transfected with Myc–lamellipodin (Myc-Lpd) and srGAP3 expression constructs. Cells were harvested the next day and immunoprecipitation was carried out using a monoclonal antibody against Myc. Precipitates were immunoblotted against srGAP3 (top) and Myc–lamellipodin (middle). The co-immunoprecipitation shows that only wild-type srGAP3 (wt) binds to Myc–lamellipodin (lane 1). The srGAP3 SH3 mutant W781A (lane 3) does not co-precipitate with Myc–lamellipodin. As a further SH3-deficient control, we introduced a Y755D mutation in the srGAP3 SH3 domain (lane 4). Y755D did not co-precipitate with lamellipodin, revealing the importance of a functional srGAP3 SH3 domain for the interaction with lamellipodin. The control lanes without antibody (Ab) incubation (lane 2) and the cell lysates transfected with srGAP3 wt (lane 5) or Myc–lamellipodin (lane 6) display no unspecific precipitates. Bottom panel is input control for srGAP3. (**B**) Total cell lysates from cultured embryonic rat cortical neurons were used in a lamellipodin immunoprecipitation using a polyclonal lamellipodin-specific antibody or control antibody. The analysis of the precipitates with an srGAP3-specific antibody indicates that the interaction between srGAP3 and lamellipodin also occurs in vivo. The control lane with an IgG control antibody shows no unspecific protein binding. Bottom panel is input control for lamellipodin. (**C**) Epifluorescent image of a mouse embryonic fibroblast cell co-transfected with EYFP–lamellipodin and mCherry–srGAP3-R542I. Both proteins show an overlapping localization at the leading edge of a protruding lamellipodium. (**D**) NIH3T3 cell co-transfected with mCherry–lamellipodin and wild-type srGAP3. Both proteins colocalize at triangular-shaped protrusions at the cell membrane (arrowhead). (**E**) Co-expression of lamellipodin and wild-type srGAP3 with constitutive-active Rac1. TIRF image showing prominent colocalization of lamellipodin and srGAP3 at the cell membrane and at the ventral cell surface. Scale bars: 10 μm (D), 25 μm (E).

interact with lamellipodin, indicating the importance of an intact SH3 domain for the interaction between srGAP3 and lamellipodin. Further evidence for an in vivo interaction between these two proteins was obtained by co-immunoprecipitation of endogenously expressed srGAP3 and lamellipodin from embryonic rat cortical neurons. The cell lysates from cultured neurons were incubated with an lamellipodin-specific antibody or an unrelated IgG. Subsequent immunoblots using specific antibodies against srGAP3 detected precipitated srGAP3 in the lamellipodin samples, but not in the control immunoprecipitations (Fig. 3B).

We also tested for co-expression of srGAP3 and lamellipodin by performing in situ hybridization on sections of the developing mouse brain. Compared with the ubiquitous expression of srGAP3 in the nervous system (Bacon et al., 2009), lamellipodin expression was more restricted. Overlapping expression of srGAP3 and lamellipodin was found, for example, in the developing pallidum and striatum at embryonic day (E)11.5 and in the hyothalamus and V and VIII ganglia at E12.5 (supplementary material Fig. S7).

Lamellipodin has been described to interact with Ena/VASP at the leading edge of protruding lamellipodia. To test whether lamellipodin and srGAP3 can both be found at the leading edge, we constructed an EYFP-tagged lamellipodin construct and expressed it together with mCherry–srGAP3 in mouse fibroblasts. Because wild-type srGAP3 strongly inhibits the formation of lamellipodia, we used the GAP-deficient R542I mutant in these experiments and found a strong overlap of both proteins at the leading edge (Fig. 3C).

We next more closely examined the colocalization of srGAP3 and lamellipodin using TIRF microscopy. As shown in Fig. 3D, wild-type srGAP3 localized at the cell membrane of small triangular-shaped protrusions that would eventually form lamellipodia. We observed the same localization for lamellipodin. Co-expression of srGAP3 and lamellipodin with constitutive-active Rac1 showed a high degree of overlap between srGAP3 and lamellipodin at the membrane and at structures close to the ventral cell surface (Fig. 3E). Similarly, using the GAP-deficient R542I mutant, we again observed a colocalization of srGAP3 and lamellipodin at the leading edge (Fig. 4A). Interestingly, in addition to the colocalization at the leading edge, we also found colocalization of srGAP3 and lamellipodin at sites of focal adhesions (Fig. 4A, arrowheads). We did not observe lamellipodin at focal adhesions when expressed alone, which is in agreement with previously published reports (Fig. 4D). In addition, we did not observe colocalization of lamellipodin with focal adhesions when it was co-expressed with the srGAP3 W781A mutant (Fig. 4B,C). We currently do not know the physiological importance of this observation, but the colocalization of lamellipodin and srGAP3 at these structures confirms the interaction of both proteins within the cell.

srGAP3 inhibits lamellipodial dynamics

srGAP3 inhibits actin polymerization by enhancing the GTPase activity of Rac1, thus averting the activation of WAVE1 (Endris et al., 2002; Soderling et al., 2002). In contrast to this, lamellipodin has been shown to increase lamellipodial dynamics by affecting the F-actin content close to the leading edge (Krause et al., 2004). The colocalization of lamellipodin and srGAP3 at sites near the cell membrane suggested the involvement of both proteins in common signaling pathways regulating actin assembly. We aimed to study srGAP3- and lamellipodin-related aspects of lamellipodia formation. For this purpose, we used the platelet-derived growth factor (PDGF) to evoke membrane protrusions at specific time points in NIH3T3 cells, because the PDGF signal transduction pathway has been well described in NIH3T3 cells (Takahashi et al., 2008; Yu et al., 2001; Li et al., 1994; Yu et al., 1994; Twamley-Stein et al., 1993).

srGAP3-overexpressing cells hardly extended lamellipodia after PDGF stimulation (Fig. 5A), whereas lamellipodin-expressing cells responded with a rapid burst of lamellipodia formation. Unlike the wild-type srGAP3 protein, the GAP-deficient srGAP3 R542I mutant responded to PDGF treatment with pronounced lamellipodia formation (Fig. 5B). This mutant shows that the repression of PDGF-induced protrusions is mainly caused by the GTPase-activating function of the GAP domain. To analyze GAP-independent effects of srGAP3 on lamellipodin and actin dynamics, we therefore included srGAP3 R542I in our studies.

To identify an srGAP3-specific effect on lamellipodin and lamellipodial dynamics or vice versa, we used live-cell imaging of PDGF-treated NIH3T3 cells transfected with srGAP3 and lamellipodin. By acquiring time-lapse movies of cells co-expressing srGAP3 (wild type and srGAP3-R542I) and lamellipodin, we tested for a functional connection between these proteins. Imaging cells co-transfected with lamellipodin and srGAP3 during PDGF stimulation revealed that, despite the overexpression of lamellipodin, lamellipodial dynamics were still downregulated, suggesting that the inhibitory effect of srGAP3 on actin dynamics is dominant over the stimulatory effect of lamellipodin. To quantify the effects of wild-type and GAP mutant srGAP3 on lamellipodin-dependent lamellipodial dynamics, we performed kymography to evaluate the velocities of lamellipodial protrusions (Hinz et al., 1999). In addition, we measured the perimeters of lamellipodia at respective protrusion peaks (Fig. 5C,D). We compared protrusion velocities of PDGF-induced lamellipodia under lamellipodin and srGAP3 (wild type and GAP mutant) single and co-expression, respectively (Fig. 5C). Within the kymograph, the slope of a protrusion (dx/dt) corresponds to the lamellipodial extension velocity (Fig. 5C′). The statistical analysis of the protrusion velocities demonstrated the strong inhibition of lamellipodial dynamics by wild-type srGAP3 and the increase in protrusion dynamics through lamellipodin overexpression compared with that in EYFP control cells (Krause et al., 2004). Co-expression of srGAP3 and lamellipodin, however, abolished the stimulatory effect of lamellipodin and even reduced the protrusion velocities below those measured in the control cells. Owing to the GAP activity of srGAP3, the inhibitory effect on lamellipodin and lamellipodial dynamics was particularly strong. The striking reduction in the protrusion velocities reflected the fact that srGAP3 generally inhibits lamellipodia formation. The co-expression of srGAP3 R542I and lamellipodin also reduced the velocity of lamellipodial protrusions although the GAP deficiency led to elevated values compared with wild-type srGAP3 expressed with lamellipodin. Furthermore, we show that srGAP3 R542I not only reduced protrusion velocities, but also diminished the stimulating effect of lamellipodin on the perimeter of outgrowing lamellipodia (Fig. 5D). Our results show that srGAP3 exerts an inhibitory effect on actin dynamics at the lamellipodia leading edge through both GAP-dependent and GAP-independent mechanisms.

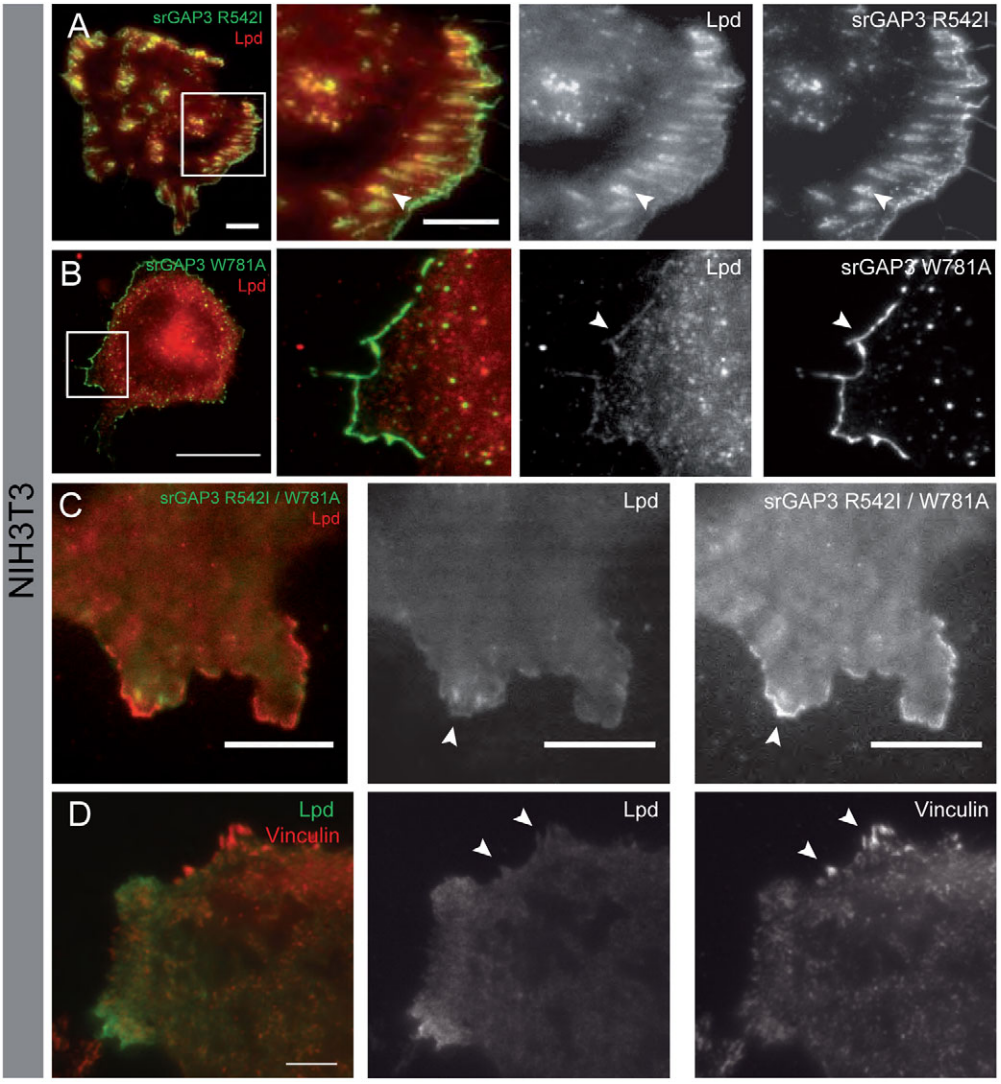

Fig. 4. srGAP3 colocalizes with lamellipodin at focal adhesions. (**A**–**C**) NIH3T3 cells were co-transfected with mCherry–lamellipodin and GAP-deficient R542I (A) or SH3 mutant (W781A) srGAP3–EYFP expression constructs (B). Similarly to the wild-type srGAP3, the GAP mutant colocalizes with lamellipodin at the cell periphery and also at focal adhesions (A, arrowheads). (B,C) SH3 mutant srGAP3 (W781A) and lamellipodin do not colocalize at specific cell structures such as focal adhesions (arrowheads). (**D**) Lamellipodin alone does not localize to focal adhesions as visualized by staining for vinculin (arrowheads). Scale bars: 10 μm (A,C), 25 μm (B), 5 μm (D).

Endogenous srGAP3 inhibits lamellipodia formation in primary fibroblasts

To investigate on the physiological role of srGAP3 on lamellipodia formation, we made use of a recently established mouse gene-knockout model of srGAP3. Embryos taken from a heterozyous *Srgap3*$^{+/-}$ × *Srgap3*$^{+/-}$ mating were individually processed and embryonic fibroblasts were cultivated. For our analyses, we only used fibroblasts at early passages (P2–P4), to enable the highest degree of comparability. First, we phenotypically analyzed cells that were grown on low-dose fibronectin (1 μg/cm^2) and 10% FCS. Quantification of cells stained with Phalloidin–TRITC showed that MEFs isolated from homozygous srGAP3-knockout animals presented an increased total cell area (wt, 2860 μm^2; *Srgap3*$^{-/-}$, 6917 μm^2; $P<0.001$), cell perimeter (wt, 381 μm; *Srgap3*$^{-/-}$, 545 μm; $P<0.01$) and number of lamellipodia compared with wild-type littermates (Fig. 6A). These data are consistent with the results obtained from our overexpression studies showing that srGAP3 is an inhibitor of actin dynamics and lamellipodia formation. Additionally, we analysed the rate of cell spreading on fibronectin. Cells were trypsinized and then plated for 15 minutes on fibronectin-coated coverslips (5 μg/cm^2) before fixation and staining with Phalloidin-TRITC. Compared with wild-type cells, the srGAP3-deficient cells spread much faster as determined by their total cell area 15 minutes after replating (wt, 1254 μm^2; *Srgap3*$^{-/-}$, 2473 μm^2; $P<0.001$; $n>300$, three independent experiments). This suggests that srGAP3 also negatively regulates cell spreading.

Next, we aimed to investigate the importance of the srGAP3–lamellipodin interaction in lamellipodiaI formation using the *Srgap3*$^{-/-}$ MEFs. We downregulated the amount of lamellipodin in *Srgap3*$^{-/-}$ MEFs using an shRNA-mediated gene-knockdown approach. For the gene knockdowns, we designed three different miR-modified shRNA molecules, cloned in a mammalian expression vector. Quantitative real-time PCR showed that these vectors resulted in a considerable gene knockdown of 36–59% for lamellipodin (supplementary material Fig. S9A). On the protein level, we could confirm the effectiveness of the gene knockdown by immunoblotting with lamellipodin-specific antibodies. We transfected the lamellipodin shRNAs into the *Srgap3*$^{-/-}$ MEFs and analyzed the cells 48 hours later. Compared with cells transfected with a control shRNA, both lamellipodin shRNAs caused an decrease in the relative cell size (percentage of lamellipodia/cell perimeter: control, 19.2%; Lpd#1, 7.8%;

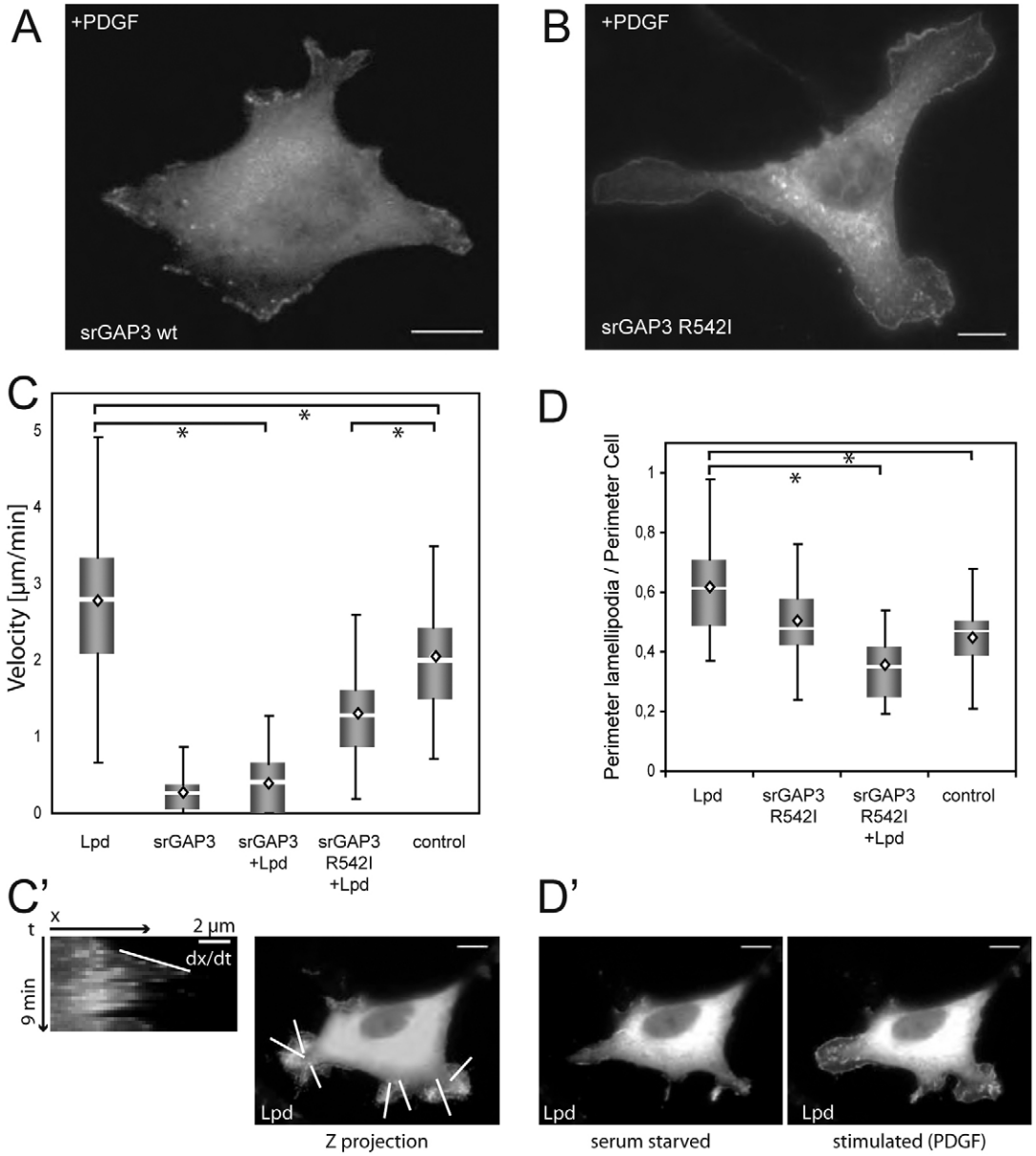

Fig. 5. srGAP3 interferes with lamellipodin-dependent lamellipodial dynamics. (**A**,**B**) Epifluorescence images of PDGF stimulated (4 minutes) NIH3T3 cells transfected with srGAP3–EYFP expression constructs and plated on fibronectin. In contrast to the wild-type srGAP3, cells transfected with the GAP-deficient srGAP3 R542I variant are able to form PDGF-induced lamellipodial protrusions. (**C**) Box and whisker plot to show protrusion velocities of primary lamellipodia after PDGF stimulation in NIH3T3 cells transfected with the indicated expression constructs for lamellipodin and srGAP3. Top and bottom boxes represent 75th and 25th quartile, and whiskers 10th and 90th percentiles, respectively. Dot indicates median and line mean values. Time-lapse movies of PDGF-treated cells were investigated by kymograph analyses in which all outgrowing lamellipodia of a stimulated cell were included. The data were obtained from at least 25 cells per transfection condition. The results reveal that srGAP3 has a pronounced inhibitory effect on lamellipodial protrusion velocities. Owing to its GAP deficiency, the srGAP3 R542I mutant (when cotransfected with lamellipodin) results in elevated velocity values compared with wild-type srGAP3 plus lamellipodin, but is still significantly lower than in control cells. (**C′**) The protrusion velocity (µm/minute) was measured from the kymograph images in which the outgrowth of the first lamellipodium (dx) against time (dt) was calculated. (**D**) Quantification of the ratio of the length of PDGF-induced lamellipodia to the length of the cell perimeter, depicted as box and whisker plot. Owing to the strong inhibitory effect of wild-type srGAP3 on protrusion formation, the influence of srGAP3 on the perimeter of lamellipodia was only investigated with the GAP-deficient srGAP3 R542I. The co-expression of srGAP3 R542I and lamellipodin not only decreases lamellipodial protrusion velocity (C), but it also diminishes the increasing effect of lamellipodin on the perimeter of formed protrusions. (**D′**) The original perimeter of the cell was measured at time 0 (serum-starved condition) and the length of lamellipodia was measured at individual protrusion peaks. Significant differences in global analysis and multiple pair-wise post-hoc comparisons with the Tukey test are indicated in C and D (*$P \leq 0.05$). Scale bars: 10 µm.

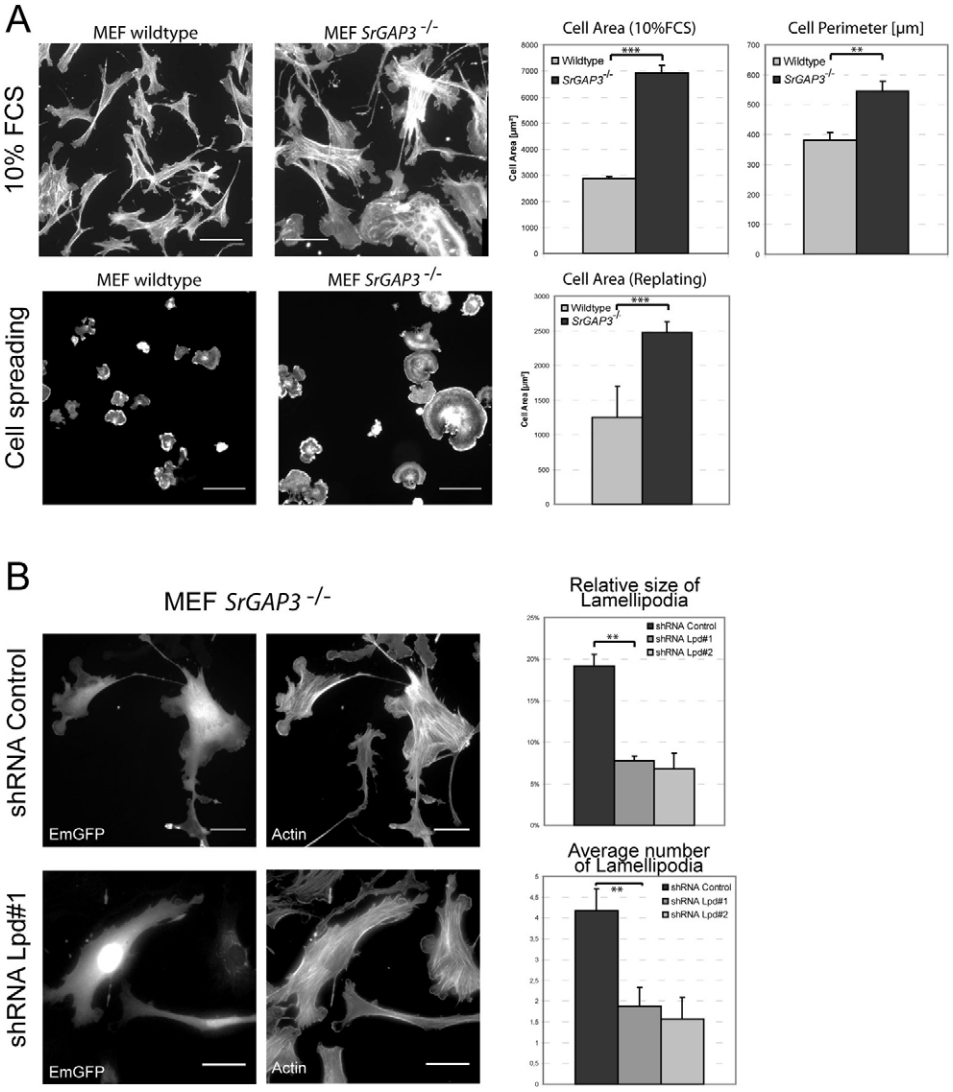

Fig. 6. srGAP3 regulates lamellipodia formation through lamellipodin in primary fibroblasts. (**A**) Analysis of mouse embryonic fibroblasts (MEFs) isolated from srGAP3-knockout embryos ($Srgap3^{-/-}$). Compared with wild-type fibroblasts isolated from the same genetic background, $Srgap3^{-/-}$ cells display a significantly increased cell area and cell perimeter as a result of an increase in the total number and size of lamellipodia. In addition, $Srgap3^{-/-}$ MEFs exhibit an increased cell spreading rate as assessed by a timed replating on fibronectin and measurement of the spread cell area. (**B**) shRNA-mediated knockdown of lamellipodin in $Srgap3^{-/-}$ MEFs diminishes the size and number of lamellipodia. $Srgap3^{-/-}$ MEFs were transfected with EmGFP-encoding shRNA plasmids (control and two different lamellipodin-shRNAs) and analyzed for F-actin 48 hours later. Both lamellipodin shRNAs, but not the control diminished the relative size of actin-rich lamellipodia at the cell front, as well as the average number of lamellipodia in these cells. Results are means ± s.e.m. $^{**}P \leq 0.01$; $^{***}P < 0.001$.

Lpd#2, 6.76%; $n > 50$, three independent experiments; $P < 0.01$) and the average number of lamellipodia per cell (control, 4.18; Lpd#1, 1.88; Lpd#2, 1.57; $P < 0.01$), indicating that srGAP3 and lamellipodin act in the same cellular pathway.

Increased process formation in N1E115 cells through srGAP3 knockdown is mediated by lamellipodin

We next examined the role of srGAP3 and lamellipodin in the neuronal-like cell line N1E-115, because both proteins are expressed in the nervous system. We observed that the overexpression of srGAP3 led to similar cell rounding effects as observed in the other studied cell lines (supplementary material Fig. S8A), whereas lamellipodin overexpression led to an increase in cell spreading, with large protrusions resembling neurites, suggesting that the increase of actin dynamics by lamellipodin overexpression affects process formation (supplementary material Fig. S8B). High-magnification images clearly showed the localization of srGAP3 and lamellipodin at the tips of dynamic filopodia (supplementary material Fig. S8C,D). Immunostaining of srGAP3 in addition showed that endogenously expressed srGAP3 also localized to the tips of filopodia in N1E-115 cells (supplementary material Fig. S8E).

A knockdown of srGAP2 in this cell line has been described to increase the number of filopodia directly after plating on laminin (Pertz et al., 2008). Analysis of srGAP3-knockdown cells using immunofluorescence and live imaging did not reveal any increase in filopodia or lamellipodia (data not shown). After incubation for 48 hours on laminin, the N1E-115 cells formed long processes resembling primary neurites. Under these conditions, we observed a significant increase in neurite-bearing cells in srGAP3-knockdown cells compared with shRNA controls (51.51% vs 28.71; $P < 0.001$) (supplementary material Fig. S9B,C), suggesting that srGAP3 negatively controls process formation. This is in agreement with a role of srGAP3 in neurite extension, because overexpression of srGAP3 in primary neurons reduces axonal length (Soderling et al., 2002). Recently, knockdown of lamellipodin has also been described to shorten axonal projections (Michael et al., 2010). Therefore, we quantified the number of neurite-bearing N1E-115 cells transfected with the knockdown constructs for srGAP3 (supplementary material Fig. S9A) or lamellipodin alone, or in combination. Whereas knockdown of lamellipodin alone did not have a statistically significant effect, we found that double knockdown efficiently rescued the stimulating effect of srGAP3

on neurite-bearing cells ($P<0.001$). Our results therefore suggest that endogenous srGAP3 and lamellipodin act together in a common pathway controlling actin dynamics, which might eventually regulate the formation of neurite-like projections in N1E-115 cells.

Discussion

In this report, we have shown that srGAP3 acts as a general inhibitor of actin dynamics at the crossroads between upstream guidance signals and key regulators of the actin machinery. In addition to the reported inhibition of Rac–WAVE signaling, we now report on a novel inhibitory function of srGAP3 through binding to lamellipodin at the cell membrane and the influence of srGAP3 on focal adhesions. We show that srGAP3 localizes to the plasma membrane through its F-BAR domain and to focal adhesions through its SH3 domain. Our results show that srGAP3 colocalizes with lamellipodin at the cell membrane, and that srGAP3 negatively regulates actin dynamics. Furthermore, we show that srGAP3 influences focal adhesion formation through the downregulation of Rac1.

F-BAR-domain-dependent membrane localization

The F-BAR domain, which is an extension of the formerly identified FCH domain (also called extended FCH or EFC domain), has been shown to be present in a variety of functionally diverse mammalian proteins (Aspenström and Kwang, 2008). One of the key aspects of F-BAR proteins is their ability to bind and deform the cell membrane, which is thought to be a priming process in either endocytotic vesicle formation or filopodia induction (Tsujita et al., 2006). In this paper, we report on the role of the F-BAR domain in targeting srGAP3 to the membrane, particularly to sites of the cell that can give rise to lamellipodial protrusions and to the tips of filopodia. The F-BAR domains of the srGAP family have recently been shown to induce filopodia-like membrane protrusions in COS7 and primary neuronal cells (Guerrier et al., 2009; Carlson et al., 2011). Interestingly, we did not observe a significant increase in filopodia number or size in NIH3T3 or B16-F1 cells expressing srGAP3. In COS7 cells, our experiments demonstrated that the observed actin-rich protrusions might be dependent on both the F-BAR and GAP domains. Thus, we conclude that the F-BAR domain of srGAP3 might facilitate actin protrusion through its membrane-bending activity. In addition, when the F-BAR domain was expressed alone, we observed several bright fluorescent spots in the cytoplasm, which might be an indication that the srGAP3 F-BAR domain is also involved in vesicle formation.

Comparing the published results from others and our own results reported here, the three mammalian members of the Slit–Robo GAP family (srGAP1–srGAP3) seem, despite their highly conserved protein architecture, to be involved in different intracellular signaling cascades. Although srGAP1 represents a GAP protein for Cdc42, both srGAP2 and srGAP3 have been shown to downregulate Rac signaling (Guerrier et al., 2009; Endris et al., 2002; Soderling et al., 2002; Wong et al., 2001). In addition, srGAP2 has been described to interact with WASP, whereas srGAP3 binds to the related WAVE1 protein. WASP is implicated in filopodia formation (Miki et al., 1998), whereas WAVE1 is more restricted to the formation of the branched actin meshwork in lamellipodia and in ruffles (Suetsugu et al., 2003; Yamazaki et al., 2005). This suggests that the three srGAP members link Slit–Robo to different signaling cascades, which is supported by the fact that they are embryonically expressed in distinct subsets of neural tissues (Bacon et al., 2009).

Interaction of srGAP3 and lamellipodin

The SH3 domain of srGAP3 has been reported previously to interact with Robo1 and WAVE1 (Soderling et al., 2002; Wong et al., 2001). To find novel interaction partners, we performed a screen using the srGAP3 SH3 domain as bait and identified several putative interaction partners. Among these, we found several proteins that are well known to be part of the WAVE complex, a multiprotein scaffold that interacts with the Arp2/3 complex and mediates branching of filamentous actin to form the underlying actin meshwork of a lamellipodium (Gautreau et al., 2004). In addition, we identified two proteins with a well-known role in actin dynamics, lamellipodin and the Ena/VASP protein Mena, which act in concert with the WAVE complex to form dynamic cell protrusions. Our further analyses showed that lamellipodin indeed constitutes a novel srGAP3 binding partner and that both proteins colocalize at the cell membrane.

Lamellipodin contains several EVH1 binding motifs that are probably recognized by the EVH1 domain of Mena (Krause et al., 2004). Intermingled with these EVH1 motifs, lamellipodin contains several SH3 binding motifs, which are most likely the sites of srGAP3 interaction. We tried to express this region of lamellipodin both in bacteria and mammalian cells, but were unable to receive a stable protein product for in vitro binding studies. Lamellipodin also contains a Ras association (RA) and a pleckstrin homology (PH) domain. Currently, the binding properties of the RA domain are not fully understood. Rodriguez-Viciana and colleagues reported on the interaction of the lamellipodin RA domain with activated forms of K-Ras, N-Ras, H-Ras and R-Ras3 using pull-down assays, whereas Krause and co-workers failed to replicate this finding using yeast two-hybrid analyses and in vitro assays using purified proteins (Rodriguez-Viciana et al., 2004; Krause et al., 2004). Additionally they were unable to show a direct interaction with Rap1 or ‘classical’ Rho-GTPases (Rho, Cdc42, Rac). However, Quinn and colleagues found an association of MIG-10, the *Caenorhabditis elegans* homolog of lamellipodin, and mammalian lamellipodin with activated Rac1 (Quinn et al., 2006). We repeated this experiment and were able to pull down lamellipodin RA using GST-bound active Rac1 (data not shown). But because pull-down experiments do not clearly distinguish between direct and indirect binding, further experiments using FRET or similar techniques are required to determine the specificity of the lamellipodin RA domain. Nonetheless, in this study we present evidence for the interaction of lamellipodin with a Rac-specific GAP protein, which suggests that lamellipodin is linked to Rac signalling. Less controversial are the findings for the PH domain, which has been shown to be important for the membrane localization of lamellipodin through binding to a specific class of phospholipids in the plasma membrane. Plasma membrane phosphoinositides have been shown to play a central role in regulating the organization and dynamics of the underlying actin cytoskeleton by acting as platforms for protein recruitment (Saarikangas et al., 2010). BAR and F-BAR domains have been implicated in sensing phosphoinositides, because they use a electrostatic interaction between positively charged residues at the outer protein surface and the negatively charged phospholipid headgroups. Indeed, the F-BAR domain of srGAP3 has been shown to interact with several membrane lipids (Carlson

et al., 2011). Thus, the PH domain of lamellipodin and the F-BAR domain of srGAP3 might both sense the plasma membrane composition to target to the leading edge of a lamellipodium.

Functionally, our data suggest that srGAP3 negatively regulates the activity of lamellipodin as shown using overexpression and gene knockout and knockdown approaches. Using live-cell imaging, we showed that srGAP3 blocks the stimulatory effect of lamellipodin on actin dynamics, particularly on protrusion formation. We propose a model, in which srGAP3 is targeted to the cell membrane through its F-BAR domain, where it interacts with lamellipodin (and/or WAVE1) and locally downregulates Rac1. This could release the interaction between Rac1 and the RA domain of lamellipodin, which in turn, might no longer be able to enhance actin dynamics at the leading edge. Together with the inhibition of WAVE1–Arp2/3-mediated actin polymerization, srGAP3 functions in blocking protrusion formation.

Further evidence for the inhibitory effect of srGAP3 on lamellipodin comes from our studies of process formation in the N1E-115 cell line. Using a knockdown approach, we found that srGAP3 is implicated in negatively regulating neurite formation. The knockdown of srGAP3 facilitated the formation of neurite-like processes, which is dependent on the presence of lamellipodin. Overexpression of lamellipodin, however, generated cells that presented lamellipodia-rich projections. These results show that srGAP3 and lamellipodin act in vivo in the same pathway. To determine whether both proteins are also involved in axon formation and elongation, further experiments using cultured primary neurons will be required.

Focal adhesion targeting of srGAP3

In this report we show that srGAP3 localizes to focal adhesions. Quantitative analyses of vinculin-positive focal adhesions indicated that the expression of srGAP3 leads to a destabilization of adhesive structures, which corresponds to our previous findings in a human neuroblastoma line (Yang et al., 2006). This effect was abolished when the GAP-deficient mutant of srGAP3 was introduced, indicating that the downregulation of Rac1 signaling plays a pivotal role. Rac1 has been shown to regulate the formation of focal contacts at the lamellipodial border, and downregulation of Rac1 through the Rac-GAP α1-chimaerin also destabilizes focal adhesions in fibroblasts (Nobes and Hall, 1995; Herrera and Shivers, 1994). The binding partner of srGAP3 at focal adhesions remains unknown. None of the three known srGAP3 binding partners (Robo1, WAVE1, lamellipodin) alone localizes to focal adhesions, raising the possibility that other srGAP3 interaction partners might exist. In view of a putative common signaling pathway, the Ena/VASP family protein Mena might be an attractive candidate, because it has been shown to interact both with lamellipodin (Krause et al., 2004) and Robo1 (Bashaw et al., 2000), and to localize to focal adhesions (Krause et al., 2003). As mentioned above, we found Mena in the list of putative interaction partners in our pull-down experiments, but further evidence is needed to confirm whether Mena is a direct or indirect binding partner of srGAP3.

Role of srGAP3 and lamellipodin in Slit–Robo signaling

Lamellipodin has previously been implicated in Slit–Robo signaling. In *C. elegans*, a homolog of lamellipodin, *MIG-10*, promotes axon guidance and outgrowth in response to the guidance cues Slit and netrin (Chang et al., 2006; Quinn et al., 2006). Mutation of *MIG-10* causes misprojection of axons in motor and mechanosensory neurons. Using in situ hybridization, we showed that srGAP3 and lamellipodin are co-expressed during embryogenesis within a subset of neural tissues. This raises the possibility that both proteins act together in a signaling cascade downstream of Slit–Robo in the processes of neuronal migration or axonal pathfinding. Recently, Michael and co-workers reported on the regulation of lamellipodin by Abl-dependent phosphorylation downstream of the attractive axon guidance cue netrin (Michael et al., 2010). The protein tyrosine kinase c-Abl has been implicated in Slit–Robo signaling, particularly in *Drosophila*, and phosphorylation of Robo through c-Abl has been reported (Bashaw et al., 2000; Rhee et al., 2002; Rhee et al., 2007). These data indicate that lamellipodin is part of the neuronal machinery regulating axon guidance. Whereas the attractive guidance cue netrin positively regulates the activity of lamellipodin (through c-Abl) leading to increased actin polymerization, the repulsive guidance cue Slit1 could negatively regulate lamellipodin through srGAP3, which in turn would locally destabilize actin filaments in the growth cone. Both srGAP3 and lamellipodin can be found in axonal growth cones, especially at the tips of filopodia, where Robo1 is also localized (unpublished observation) (Krause et al., 2004).

Our data suggest that the different domains of srGAP3 might work together to implement the protein in a signaling cascade downstream of Robo1. In the neuronal growth cone, the F-BAR domain might localize srGAP3 to the leading edge, where it interacts with Robo1 through its SH3 domain. Slit binding to the Robo receptor might initiate a signaling pathway leading to activation of the srGAP3 GAP activity. Downregulation of the Rac1–WAVE1 signaling complex, local destabilization of focal contacts and the inhibition of lamellipodin–Mena might then lead to the necessary inhibition of actin dynamics in the growth cone necessary for turning away from Slit.

Materials and Methods

cDNA expression constructs

The full-length open reading frames of human srGAP3 isoforms a (NM_014850) and b (NM_001033117) were cloned in pcDNA4/TO/mycHis or pENTR vector (Invitrogen). The EYFP- or mCherry-tagged srGAP3 expression vectors were generated by cloning EYFP C-terminally, thereby eliminating the stop codon. Point mutations (R542I, W781A, Y755D) were introduced using site-directed mutagenesis (Stratagene). The F-BAR-deleted construct was generated from pENTR-srGAP3a by deleting amino acids 7–407 and shuttling into pDEST-NT-YFP vector. The F-BAR-only construct encompassing amino acids 1–573 of srGAP3a was generated in pENTR vector and shuttled into pDEST-NT-YFP.

GST-tagged constructs for bacterial expression and fusion protein purification were generated in pGEX4T vectors (GE Healthcare). A human *LPD* (accession NM_213589) expression construct encoding the full-length open reading frame was generated in a pENTR vector (Invitrogen) with the expression clone KIAA1681 (Kazusa Institute) and by amplifying the N-terminal part of *LPD* from the RZPD clone IRAK p961N1864Q2 (hLpd_Start_Sal_for, 5′-GCAGTCGACATGGAGCAGCTATCAGATGGA-3′; hLpd_467_rev, 5′-AGGC-ATCCAGATCCACAGTC-3′).

Antibodies

The polyclonal antibody against srGAP3 (19.1) was raised in rabbit using synthetic peptides (N-CHELRELERQNTVKQ-C) fused to KLH corresponding to amino acids 973–985 of the human full-length srGAP3a protein. The antibody was purified over a srGAP3-peptide-conjugated Sepharose 4B column (Pineda Antibody Service, Berlin, Germany). Specificity of the antibody was checked on western blots and by immunofluorescence. No signal was observed when the antibody was cross-absorbed with the respective peptides used for immunization. For immunofluorescence studies, commercially available polyclonal antibodies against the srGAP3 C-terminus were used (Sigma, S1575; SAB4200050). Specificity of both antibodies was tested by staining sections of *Srgap3*$^{-/-}$ embryos. The antibody against the Myc tag was purchased from Cell Signaling Technology (monoclonal, 9B11). Monoclonal anti-vinculin hVIN-1 was

from Sigma. The antibody against lamellipodin was a kind gift from Frank Gertler (Krause et al., 2004). Secondary antibodies conjugated to Alexa Fluor 350, 488 or 568, for immunofluorescence staining, were obtained from Invitrogen.

Cell culture

HEK293, NIH3T3 and COS7 were cultured in DMEM high glucose (Invitrogen), supplemented with 10% fetal (for HEK293, Cos7) or newborn (for NIH3T3) calf serum and penicillin-streptomycin, at 37℃ and 5% CO_2. N1E-115 neuroblastoma cells (ECACC, #88112303) were cultured in Dulbecco's modified Eagle's medium (DMEM) (supplemented with 10% fetal calf serum, 1% non-essential amino acids, 1% penicillin-streptomycin) at 37℃ and 5% CO_2. Mouse embryonic fibroblasts were prepared from E14.5 embryos of a $Srgap3^{+/-} \times Srgap3^{+/-}$ mating. Embryos were individually processed and subsequently genotyped. For all analyses, only early passages (P2–P4) were used. For shRNA transfection, 4×10^5 cells were nucleofected with 4 µg DNA using Amaxa nucleofector program A-23 according to the manufacturer (Lonza) and plated on fibronectin-coated glass coverslips in 24-well plates. Cells were fixed 48 hours later and processed for immunostaining.

Immunoprecipitation and pull-down assays

Immunoprecipitations were carried out using standard procedures. Transiently transfected HEK293 cells, cultured neurons or freshly isolated adult mouse brain were lysed in modified RIPA buffer (50 mM Tris-HCl, pH 7.4, 150 mM NaCl, 1% NP-40, 0.25% sodium deoxycholate, 1 mM EDTA, 2 mM Na_3VO_4, 2 mM NaF) supplemented with protease inhibitor mix G (Serva). Immunocomplexes were precipitated using Ultralink Protein A/G Sepharose (Pierce), separated by SDS-Page together with 20 µg of total cell extracts as control and blotted onto PVDF membranes (for detection with ECL solution: Hybond-P, GE Healthcare; for LI-COR imager: Immobilon-FL, Millipore). Western blots were blocked with 3% milk in 1× TBS-T or with 50% Odyssey Blocking Buffer in 1× TBS and incubated with primary antibody solutions in blocking buffer including 0.1% Tween. Membranes were washed in 1× TBS-T followed by secondary antibody incubation (ECL detection: HRP-conjugated, LI-COR imager: fluorophore-labelled IRDye 680 and 800CW) in blocking buffer. Blots were developed using the Supersignal Pico reagent (Pierce) or scanned with a LI-COR imager for quantitative analyses.

Immunofluorescence

NIH3T3 cells were plated on Fibronectin-coated (5–10 µg/cm^2, Bovine Plasma Fibronectin, Invitrogen) four-well LabTek II chambered coverglass slides overnight and cultured in Opti-MEM I with 10% newborn calf serum. Cells were transfected with the Lipofectamine 2000 reagent according to the manufacturer. Four hours after transfection, medium was replaced with Opti-MEM I supplemented with 0.1% newborn calf serum and penicillin-streptomycin. Cells were serum-starved over night and either used for live-cell imaging or fixed in 4% paraformaldehyde and 4% sucrose in 1× PBS at 37℃ for 10 minutes. After PBS washes, cells were permeabilized in 1×PBS with 0.1% Tween (PBS-T). After blocking with 3% BSA in PBS-T cells were incubated with primary antibodies overnight at 4℃ in 1% BSA in PBS-T. Cells were then washed in PBS-T, blocked and incubated with secondary antibodies at room temperature for 1 hour.

Fluorescence microscopy and live-cell imaging

Fixed and live cells were imaged on a Nikon ECLIPSE Ti with either Nikon 60× PlanApo TIRF NA 1.45 or Nikon 100× PlanApo TIRF NA 1.45 objective lenses. Images for EYFP, mCherry and DIC contrast were acquired with a Hamamatsu ORCA-AG high-resolution CCD camera using the NIS-Elements 3.0 software. Live-cell imaging was performed with implementation of the Nikon Perfect Focus system. During acquisition of time-lapse movies, cells were kept in Opti-MEM I supplemented with 0.1% newborn calf serum, penicillin-streptomycin and incubated at 37℃ in 5% CO_2 using a Tokai Hit environmental chamber. The stimulation of lamellipodia was induced by adding PDGF-BB (Invitrogen) on stage at a concentration of 100 ng/ml at imaging time zero. Images and movies were processed with NIS-Elements 3.0, ImageJ and Photoshop.

Focal adhesion measurement

For quantification of focal adhesions, formaldehyde-fixed cells transfected with EYFP-tagged srGAP3 constructs were immunostained using a monoclonal anti-vinculin antibody (Sigma) and anti-mouse Alexa Fluor 568 secondary antibody. TIRF images from random fields were acquired of more than 100 cells for each condition. The number and size of focal adhesions was determined using the 'Particle analysis' function in ImageJ in thresholded images (Komatsu and Ikebe, 2007).

Cell spreading measurement

For the analysis of cell spreading, wild-type and srGAP3-knockout MEFs were trypsinized simultaneously and resuspended in normal growth medium containing soybean trypsin inhibitor. The cells were then plated on coverslips coated with 5 µg/cm^2 and allowed to adhere and spread for 15 minutes. Cells were then quickly fixed in prewarmed 3.7% paraformaldehyde and analyzed using immunofluorescence. The total spread cell area and cell perimeter were measured using ImageJ.

Kymograph analysis

Time-lapse movies of transfected NIH3T3 cells under PDGF stimulation were analyzed by drawing a line one pixel in width at a 90° angle across a lamellipodium in the direction of protrusion (Krause et al., 2004). According to the SACED method (Hinz et al., 1999) and by using a kymograph macro for ImageJ, the image from this line was copied from each frame of the movie and pasted along the x axis to generate a composite kymograhic image. We measured the slope of primary protrusion peaks (dx/dt) and thereby calculated lamellipodial protrusion velocities (µm/minute).

Statistical analyses

Statistical analysis for protrusion velocities and perimeter ratios was performed with SAS V9.1 for windows using a generalized linear model with repeated measurements. Global tests and multiple pair-wise post-hoc comparisons with the Tukey test were performed holding the global 5% error level. Cell area, focal adhesion and neurite outgrowth measurements were analyzed using standard Student's t-test or one-way ANOVA analyses. Statistical significance was assumed when $P<0.01$.

shRNA-mediated knockdown

For the gene knockdown studies, we used the Block-it Pol II miR RNAi System (Invitrogen), which includes a pcDNA6.2 vector expressing EmGFP in cis with a miR-modified shRNA oligo. For srGAP3 and lamellipodin, three different shRNAs were designed using the algorithm from the manufacturer. The oligo sequences can be found in the supplementary material Table S1. For double knockdowns, we exchanged the EmGFP with mCherry using *Dra*I restriction. Functionality of the shRNAs was tested by expression of the vectors in the N1E-115 cell line and subsequent real-time PCR on a 7500 Fast Real-Time PCR machine (Applied Biosystems). Expression levels of srGAP3 and lamellipodin were normalized against two different housekeeping genes.

For the analysis of neurite outgrowth, N1E-115 cells were seeded onto laminin-coated coverslips and transfected using Lipofectamine 2000 (Invitrogen) according to the manufacturer's instructions. To induce process outgrowth, cells were cultured with Neurite Outgrowth medium (Millipore) (supplemented with L-glutamine and penicillin-streptomycin) for 42 hours. N1E-115 cells were then fixed for 15 minutes with 4% paraformaldehyde in 4% sucrose at 37℃. For actin staining, the N1E-115 cells were permeabilized with 0.5% NP40 (in 1× PBS) for 5 minutes and then incubated in TRITC-conjugated phalloidin for 45 minutes. Cells were counterstained with DAPI (2 mg/ml) for 3 minutes to detect nuclei.

GST pull-down

For the pull-down experiments, GST fusion proteins containing the srGAP3 SH3 domain were mixed with extracts from transiently transfected HEK293 cells or adult mouse brain (in modified RIPA) and incubated overnight at 4℃ on a rotator. Unbound proteins were washed off with RIPA buffer and complexes with GST–srGAP3-SH3 and interacting proteins were analyzed via SDS-PAGE and western blot. Proteins that were pulled down together with GST–srGAP3-SH3 were analyzed, after trypsin digestion, in an ESI-QUAD-TOF instrument to obtain the MS/MS fragment ion masses. The data obtained from MS/MS were analyzed by the Mascot program and compared with mammalian sequences from the NCBInr protein database.

In situ hybridization

Embryo fixation, embedding, cryosectioning and in situ hybridization were performed as described (Bacon et al., 2009) with some modifications. Before hybridization, the slides were treated for 10 minutes with 5 µg/ml proteinase K, followed by post-fixation with 4% paraformaldehyde to inactivate the proteinase K. The slides were then treated with 0.1 M RNase-free triethanolamine-HCl, pH 8.0, to remove charge on the slide and decrease background binding of the negatively charged RNA probe. Post-hybridization steps were performed as previously described with the exception that slides were washed in a formamide-free wash buffer.

The probe for lamellipodin was constructed by amplifying a 561 bp fragment from the 5′ end of the mouse *Lpd* gene using primers mLpd_Ex1_for: 5′-GGACCTGGATAAAATGTTTGGG-3′ and mLpd_827_rev: 5′-CGGGAGGAG-TTACTGATGGA-3′. The amplified product was cloned into pST-blue vector (Novagen) and in vitro translated using SP6 and T3 as described.

Acknowledgements

We thank Robert Waltereit and Dusan Bartsch for the generation of the srGAP3-knockout mice, Frank Gertler for the generous gift of the

lamellipodin antibody and Ulrike Engel from the Heidelberg Nikon imaging center for support in microscopy.

Funding

This work was supported by grant SFB488 and graduate college GK791 from the Deutsche Forschungsgesellschaft.

Supplementary material available online at
http://jcs.biologists.org/lookup/suppl/doi:10.1242/jcs.077081/-/DC1

References

Applewhite, D. A., Barzik, M., Kojima, S., Svitkina, T. M., Gertler, F. B. and Borisy, G. G. (2007). Ena/VASP proteins have an anti-capping independent function in filopodia formation. *Mol. Biol. Cell* **18**, 2579-2591.

Aspenström, P. and Kwang, W. J. (2008). Roles of F-BAR/PCH proteins in the regulation of membrane dynamics and Actin reorganization. *Int. Rev. Cell. Mol. Biol.* **272**, 1-31.

Bacon, C., Endris, V. and Rappold, G. (2009). Dynamic expression of the Slit-Robo GTPase activating protein genes during development of the murine nervous system. *J. Comp. Neurol.* **513**, 224-236.

Bashaw, G. J., Kidd, T., Murray, D., Pawson, T. and Goodman, C. S. (2000). Repulsive axon guidance: Abelson and Enabled play opposing roles downstream of the roundabout receptor. *Cell* **101**, 703-715.

Brose, K., Bland, K. S., Wang, K. H., Arnott, D., Henzel, W., Goodman, C. S., Tessier-Lavigne, M. and Kidd, T. (1999). Slit proteins bind Robo receptors and have an evolutionarily conserved role in repulsive axon guidance. *Cell* **96**, 795-806.

Carlson, B. R., Lloyd, K. E., Kruszewski, A., Kim, I. H., Rodriguiz, R. M., Heindel, C., Faytell, M., Dudek, S. M., Wetsel, W. C. and Soderling, S. H. (2011). WRP/srGAP3 facilitates the initiation of spine development by an inverse F-BAR domain, and its loss impairs long-term memory. *J. Neurosci.* **31**, 2447-2460.

Chang, C., Adler, C. E., Krause, M., Clark, S. G., Gertler, F. B., Tessier-Lavigne, M. and Bargmann, C. I. (2006). MIG-10/Lamellipodin and AGE-1/PI3K promote axon guidance and outgrowth in response to Slit and Netrin. *Curr. Biol.* **16**, 854-862.

Drees, F. and Gertler, F. B. (2008). Ena/VASP: proteins at the tip of the nervous system. *Curr. Opin. Neurobiol.* **18**, 53-59.

Eden, S., Rohatgi, R., Podtelejnikov, A. V., Mann, M. and Kirschner, M. W. (2002). Mechanism of regulation of WAVE1-induced actin nucleation by Rac1 and Nck. *Nature* **418**, 790-793.

Endris, V., Wogatzky, B., Leimer, U., Bartsch, D., Zatyka, M., Latif, F., Maher, E. R., Tariverdian, G., Kirsch, S., Karch, D. and Rappold, G. A. (2002). The novel Rho-GTPase activating gene MEGAP/ srGAP3 has a putative role in severe mental retardation. *Proc. Natl. Acad. Sci. USA* **99**, 11754-11759.

Gautreau, A., Ho, H. Y., Li, J., Steen, H., Gygi, S. P. and Kirschner, M. W. (2004). Purification and architecture of the ubiquitous Wave complex. *Proc. Natl. Acad. Sci. USA* **101**, 4379-4383.

Geraldo, S. and Gordon-Weeks, P. R. (2009). Cytoskeletal dynamics in growth-cone steering. *J. Cell Sci.* **122**, 3595-3604.

Guerrier, S., Coutinho-Budd, J., Sassa, T., Gresset, A., Jordan, N. V., Chen, K., Jin, W. L., Frost, A. and Polleux, F. (2009). The F-BAR domain of srGAP2 induces membrane protrusions required for neuronal migration and morphogenesis. *Cell* **138**, 990-1004.

Hall, A. (1998). Rho GTPases and the Actin cytoskeleton. *Science* **279**, 509-514.

Heath, R. J. W. and Insall, R. H. (2008). F-BAR domains: multifunctional regulators of membrane curvature. *J. Cell. Sci.* **121**, 1951-1954.

Herrera, R. and Shivers, B. D. (1994). Expression of alpha-1-chimaerin (rac-1 GAP) alters the cytoskeletal and adhesive properties of fibroblasts. *J. Cell. Biochem.* **56**, 582-591.

Hinz, B., Alt, W., Johnen, C., Herzog, V. and Kaiser, H. W. (1999). Quantifying lamella dynamics of cultured cells by SACED, a new computer-assisted motion analysis. *Exp. Cell Res.* **251**, 234-243.

Hohenester, E. (2008). Structural insight into Slit-Robo signalling. *Biochem. Soc. Trans.* **36**, 251-256.

Itoh, T. and De Camilli, P. (2006). BAR, F-BAR (EFC) and ENTH/ANTH domains in the regulation of membrane-cytosol interfaces and membrane curvature. *Biochim. Biophys. Acta.* **1761**, 897-912.

Komatsu, S. and Ikebe, M. (2007). The phosphorylation of Myosin II at the Ser1 and Ser2 is critical for normal Platelet-derived Growth Factor induced reorganization of Myosin filaments. *Mol. Biol. Cell* **18**, 5081-5090.

Krause, M., Dent, E. W., Bear, J. E., Loureiro, J. J. and Gertler, F. B. (2003). ENA/VASP PROTEINS: Regulators of the Actin cytoskeleton and cell migration. *Annu. Rev. Cell Dev. Biol.* **19**, 541-564.

Krause, M., Leslie, J. D., Stewart, M., Lafuente, E. M., Valderrama, F., Jagannathan, R., Strasser, G. A., Rubinson, D. A., Liu, H., Way, M., Yaffe, M. B., Boussiotis, V. A. and Gertler, F. B. (2004). Lamellipodin, an Ena/VASP ligand, is implicated in the regulation of lamellipodial dynamics. *Dev. Cell* **7**, 571-583.

Li, W., Yu, J. C., Michieli, P., Beeler, J. F., Ellmore, N., Heidaran, M. A. and Pierce, J. H. (1994). Stimulation of the platelet-derived growth factor beta receptor signaling pathway activates protein kinase C-delta. *Mol. Cell. Biol.* **14**, 6727-6735.

McPherson, V. A., Everingham, S., Karisch, R., Smith, J. A., Udell, C. M., Zheng, J., Jia, Z. and Craig, A. W. B. (2009). Contributions of F-BAR and SH2 domains of Fes protein tyrosine kinase for coupling to the FcεRI pathway in mast cells. *Mol. Cell. Biol.* **29**, 389-401.

Mellor, H. (2010). The role of formins in filopodia formation. *Biochim. Biophys. Acta.* **1803**, 191-200.

Michael, M., Vehlow, A., Navarro, C. and Krause, M. (2010). c-Abl, Lamellipodin, and Ena/VASP proteins cooperate in dorsal ruffling of fibroblasts and axonal morphogenesis. *Curr. Biol.* **20**, 1-9.

Miki, H., Sasaki, T., Takai, Y. and Takenawa, T. (1998). Induction of filopodium formation by a WASP-related actin-depolymerizing protein N-WASP. *Nature* **391**, 93-96.

Nguyen-Ba-Charvet, K. T. and Chédotal, A. (2002). Role of Slit proteins in the vertebrate brain. *J. Physiol.* **96**, 91-98.

Nobes, C. D. and Hall, A. (1995). Rho, Rac, and Cdc42 GTPases regulate the assembly of multimolecular focal complexes associated with actin stress fibers, lamellipodia, and filopodia. *Cell* **81**, 53-62.

Nobes, C. D., Hawkins, P., Stephens, L. and Hall, A. (1995). Activation of the small GTP-binding proteins rho and rac by growth factor receptors. *J. Cell. Sci.* **108**, 225-233.

Pertz, O. C., Wang, Y., Yang, F., Wang, W., Gay, L. J., Gristenko, M. A., Clauss, T. R., Anderson, D. J., Liu, T., Auberry, K. J., Camp, D. G., II, Smith, R. D. and Klemke, R. L. (2008). Spatial mapping of the neurite and soma proteomes reveals a functional Cdc42/Rac regulatory network. *Proc. Natl. Acad. Sci. USA* **105**, 1931-1936.

Quinn, C. C., Pfeil, D. S., Chen, E., Stovall, E. L., Harden, M. V., Gavin, M. K., Forrester, W. C., Ryder, E. F., Soto, M. C. and Wadsworth, W. G. (2006). UNC-6/Netrin and SLT-1/Slit guidance cues orient axon outgrowth mediated by MIG-10/RIAM/Lamellipodin. *Curr. Biol.* **16**, 845-853.

Rhee, J., Mahfooz, N. S., Arregui, C., Lilien, J., Balsamo, J. and VanBerkum, M. F. (2002). Activation of the repulsive receptor Roundabout inhibits N-cadherin-mediated cell adhesion. *Nat. Cell Biol.* **4**, 798-805.

Rhee, J., Buchan, T., Zukerberg, L., Lilien, J. and Balsamo, J. (2007). Cables links Robo-bound Abl kinase to N-cadherin-bound beta-catenin to mediate Slit-induced modulation of adhesion and transcription. *Nat. Cell Biol.* **9**, 883-892.

Rodriguez-Viciana, P., Sabatier, C. and McCormick, F. (2004). Signaling specificity by Ras Family GTPases is determined by the full spectrum of effectors they regulate. *Mol. Cell. Biol.* **24**, 4943-4954.

Saarikangas, J., Zhao, H. and Lappalainen, P. (2010). Regulation of the Actin cytoskeleton-plasma membrane interplay by phosphoinositides. *Physiol. Rev.* **90**, 259-289.

Shimada, A., Niwa, H., Tsujita, K., Suetsugu, S., Nitta, K., Hanawa-Suetsugu, K., Akasaka, R., Nishino, Y., Toyama, M., Chen, L. et al. (2007). Curved EFC/F-BAR-domain dimers are joined end to end into a filament for membrane invagination in endocytosis. *Cell* **129**, 761-772.

Soderling, S. H., Binns, K. L., Wayman, G. A., Davee, S. M., Ong, S. H., Pawson, T. and Scott, J. D. (2002). The WRP component of the WAVE-1 complex attenuates Rac-mediated signaling. *Nat. Cell Biol.* **4**, 970-975.

Soderling, S. H., Guire, E. S., Kaech, S., White, J., Zhang, F., Schutz, K., Langeberg, L. K., Banker, G., Raber, J. and Scott, J. D. (2007). A WAVE-1 and WRP signaling complex regulates spine density, synaptic plasticity, and memory. *J. Neurosci.* **27**, 355-365.

Stradal, T. E. B. and Scita, G. (2006). Protein complexes regulating Arp2/3-mediated actin assembly. *Curr. Opin. Cell Biol.* **18**, 4-10.

Suetsugu, S., Yamazaki, D., Kurisu, S. and Takenawa, T. (2003). Differential roles of WAVE1 and WAVE2 in dorsal and peripheral ruffle formation for fibroblast cell migration. *Dev. Cell* **5**, 595-609.

Takahashi, M., Rikitake, Y., Nagamatsu, Y., Hara, T., Ikeda, W., Hirata, K. and Takai, Y. (2008). Sequential activation of Rap1 and Rac1 small G proteins by PDGF locally at leading edges of NIH3T3 cells. *Genes Cells* **13**, 549-569.

Toguchi, M., Richnau, N., Ruusala, A. and Aspenström, P. (2010). Members of the CIP4 family of proteins participate in the regulation of platelet-derived growth factor receptor-beta-dependent actin reorganization and migration. *Biol. Cell* **102**, 215-230.

Tokuo, H. and Ikebe, M. (2004). Myosin X transports Mena/VASP to the tip of filopodia. *Biochem. Biophys. Res. Commun.* **319**, 214-220.

Tsujita, K., Suetsugu, S., Sasaki, N., Furutani, M., Oikawa, T. and Takenawa, T. (2006). Coordination between the actin cytoskeleton and membrane deformation by a novel membrane tubulation domain of PCH proteins is involved in endocytosis. *J. Cell Biol.* **172**, 2269-2279.

Twamley-Stein, G. M., Pepperkok, R., Ansorge, W. and Courtneidge, S. A. (1993). The Src family tyrosine kinases are required for platelet-derived growth factor-mediated signal transduction in NIH 3T3 cells. *Proc. Natl. Acad. Sci. USA* **90**, 7696-7700.

Wong, K., Ren, X. R., Huang, Y. Z., Xie, Y., Liu, G., Saito, H., Tang, H., Wen, L., Brady-Kalnay, S. M., Mei, L., Wu, J. Y., Xiong, W. C. and Rao, Y. (2001). Signal transduction in neuronal migration: roles of GTPase activating proteins and the small GTPase Cdc42 in the Slit-Robo pathway. *Cell* **107**, 209-221.

Yamazaki, D., Fujiwara, T., Suetsugu, S. and Takenawa, T. (2005). A novel function of WAVE in lamellipodia: WAVE1 is required for stabilization of lamellipodial protrusions during cell spreading. *Genes Cells* **10**, 381-392.

Yang, Y., Marcello, M., Endris, V., Saffrich, R., Fischer, R., Trendelenburg, M. F., Sprengel, R. and Rappold, G. (2006). MEGAP impedes cell migration via regulating actin and microtubule dynamics and focal complex formation. *Exp. Cell Res.* **312**, 2379-2393.

Yu, J., Moon, A. and Kim, H. R. (2001). Both platelet-derived growth factor receptor (PDGFR)-alpha and PDGFR-beta promote murine fibroblast cell migration. *Biochem. Biophys. Res. Commun.* **282**, 697-700.

Yu, J. C., Gutkind, J. S., Mahadevan, D., Li, W., Meyers, W. A., Pierce, J. H. and Heidaran, M. A. (1994). Biological function of PDGF-induced PI-3 kinase activity: its role in alpha PDGF receptor-mediated mitogenic signaling. *J. Cell Biol.* **127**, 479-487.

Yu, T. W., Hao, J. C., Lim, W., Tessier-Lavigne, M. and Bargmann, C. I. (2002). Shared receptors in axon guidance: SAX-3/Robo signals via UNC-34/Enabled and a Netrin-independent UNC-40/DCC function. *Nat. Neurosci.* **5**, 1147-1154.

Journal of Cell Science

Table S1. Oligonucleotides used for shRNA-mediated gene knock-down

shRNA name	Oligonucleotide name	Sequence (5'_ 3')
srGAP3#1	NM_080448_2254_top	TGCTGTATGGCTATACACTGAAAGAGGTTTTGG
		CCACTGACTGACCTCTTTCAGTATAGCCATA
	NM_080448_2254_bottom	CCTGTATGGCTATACTGAAAGAGGTCAGTCAGT
		GGCCAAAACCTCTTTCAGTGTATAGCCATAC
srGAP3#2	NM_080448_2289_top	TGCTGCTTAATGAACGCTTCCATACTGTTTTGGC
		CACTGACTGACAGTATGGACGTTCATTAAG
	NM_080448_2289_bottom	CCTGCTTAATGAACGTCCATACTGTCAGTCAGTG
		GCCAAAACAGTATGGAAGCGTTCATTAAGC
srGAP3#3	NM_080448_3157_top	TGCTGTGTCCTGTACAACTATGTACTGTTTTGGC
		CACTGACTGACAGTACATATGTACAGGACA
	NM_080448_3157_bottom	CCTGTGTCCTGTACATATGTACTGTCAGTCAGTG
		GCCAAAACAGTACATAGTTGTACAGGACAC
Lpd#1	Mmi579421_top_Raph1	TGCTGATTAGAGGAAGATGACGGTCCGTTTTGG
		CCACTGACTGACGGACCGTCCTTCCTCTAAT
	Mmi579421_bot_Raph1	CCTGATTAGAGGAAGGACGGTCCGTCAGTCAGT
		GGCCAAAACGGACCGTCATCTTCCTCTAATC
Lpd#2	Mmi579422_top_Raph1	TGCTGTCCGCTGTCAGACTGATTAGAGTTTTGGC
		CACTGACTGACTCTAATCACTGACAGCGGA
	Mmi579422_bot_Raph1	CCTGTCCGCTGTCAGTGATTAGAGTCAGTCAGTG
		GCCAAAACTCTAATCAGTCTGACAGCGGAC
Lpd#3	Mmi579423_top_Raph1	TGCTGTATACTGAGACTTCTTCTGGAGTTTTGGC
		CACTGACTGACTCCAGAAGGTCTCAGTATA
	Mmi579423_bot_Raph1	CCTGTATACTGAGACCTTCTGGAGTCAGTCAGTG
		GCCAAAACTCCAGAAGAAGTCTCAGTATAC